AN ANALYTIC-GEOMETRIC MODEL OF THE EFFECT OF SPHERICALLY DISTRIBUTED INJECTION ERRORS FOR GALILEO AND ULYSSES SPACECRAFT: THE MULTI-STAGE PROBLEM*

James M. Longuski *
and
Angus D. McRonald**

Jet Propulsion Laboratory
California Institute of Technology
Pasadena, California 91109

88-4245-CP

Abstract

In previous work the problem of injecting the Galileo and Ulysses spacecraft from low earth orbit into their respective interplanetary trajectories has been discussed for the single stage (Centaur) vehicle. The central issue, in the event of spherically distributed injection errors, is what happens to the vehicle? The difficulties addressed in this paper involve the multi-stage problem since both Galileo and Ulysses will be utilizing the two-stage IUS system. Ulysses will also include a third stage: the PAM-S. The solution is expressed in terms of probabilities for total percentage of escape, orbit decay and reentry trajectories. Analytic solutions are found for Hill's Equations of Relative Motion (more recently called Clohessy-Wiltshire Equations) for multi-stage injections. These solutions are interpreted geometrically on the injection sphere. The analytic-geometric models compare well with numerical solutions, provide insight into the behavior of trajectories mapped on the injection sphere and simplify the numerical two-dimensional search for trajectory families.

Introduction

A previous paper[1] addresses the single stage problem for Galileo and Ulysses in which the Centaur vehicle was planned to be used for both injections. The current plan is to use the IUS system, which means that the Galileo will have two stages and the Ulysses will use three stages, the third being a PAM-S. There will be time delays between stages so that the analytic solutions used in the past are invalid. An entirely new analysis is required for the multi-stage problem. The numerical method for the analysis is the same as in previous work.[2,3]

The numerical approach involves selecting a pointing direction for injection in inertial space defined by a cone angle, A, and a clock angle, B, and then numerically integrating the trajectory to find the resulting conditions. It is assumed that the misalignment of the injection can take place anywhere on the sphere. The probability associated with each identified case is found by numerical integration over the sphere. The types of cases identified are escape trajectories, powered entries (entry while the vehicle is still thrusting), orbit decay and prompt and delayed entries. Several points must be selected on the sphere in order to obtain enough results to accurately categorize the reentry types and to assign probabilities.

The main problem with the numerical approach is that it is tedious and time consuming. The goal of this paper is to generalize the analytic-geometric models of the previous paper to include the multi-stage case. Before discussing the multi-stage case, the impulsive injection and single stage cases will be reviewed.

The Velocity Sphere for Impulsive Injection from Circular Orbit

Fig. 1 illustrates the velocity sphere of all possible injection orientations from circular orbit. The radius of the sphere is equal to a constant, V_I. For a specific injection the orientation of V_I is defined by a cone angle, A, and a clock angle, B. Note that these angles are analogous to co-latitude (for A) and longitude (for B). If the cone angle A is zero, then the injection velocity is aligned with the circular velocity vector and the vehicle achieves its maximum energy. A cone angle of 180° will result in the minimum energy. Clearly the cone angle, A, determines the orbital energy the vehicle receives. The clock angle, B, determines the angular momentum (to be shown later). For a given value of A, B = 90° will result in the maximum flight path angle, while B = -90° corresponds to the minimum.

The Escape Cone in the AB Plane. We will now consider the escape trajectories resulting from spherically distributed injection errors.

Fig. 2 illustrates the escape cone resulting from such a simple model. Since

$$V_{esc} = 2^{1/2} V_c \tag{1}$$

and from the law of cosines

$$V_{esc}^2 = V_c^2 + V_I^2 + 2V_c V_I \cos A_{esc} \tag{2}$$

we obtain from Eqs. 1 and 2

$$A_{esc} = \cos^{-1}\left[\left(V_c^2 - V_I^2\right)/2V_c V_I\right] \tag{3}$$

The fractional area, S_{esc}, encompassed by the escape cone is given by

$$S_{esc} = (1 - \cos A_{esc})/2 \tag{4}$$

In the AB plane the escape cone appears as a straight line, as shown in Fig. 3.

*The research described in this paper was carried out by the Jet Propulsion Laboratory, California Institute of Technology under contract with the National Aeronautics and Space Administration.
**Members of Technical Staff, Mission Design Section, Jet Propulsion Laboratory, California Institute of Technology.

Copyright © American Institute of Aeronautics and Astronautics, Inc., 1988. All rights reserved.

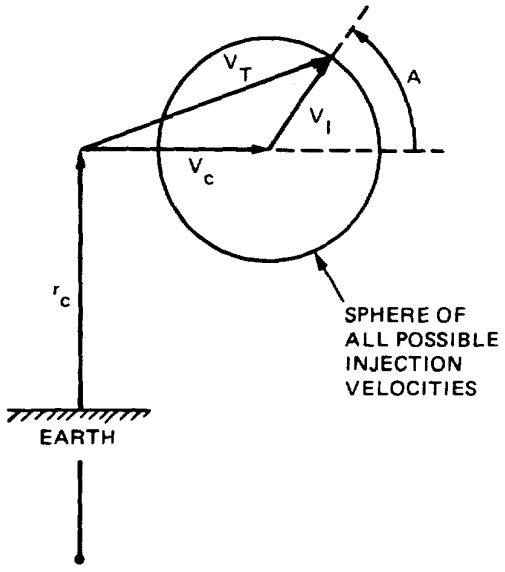

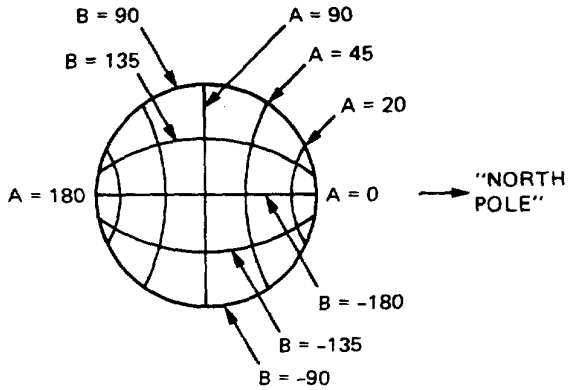

COORDINATE SYSTEM FOR V_I

A = CONE ANGLE (CO-LATITUDE)

B = CLOCK ANGLE (LONGITUDE)

Fig. 1. Coordinate system for velocity sphere

In Fig. 2 all trajectories with cone angles less than or equal to A_{esc} have the necessary energy for escape. However, not all of these cases result in actual escape because those having negative flight path angles may reenter before or during the pass through periapsis. For low Earth orbit, nearly half of the trajectories with escape energy will reenter.

Thus, a more complex problem arises, namely the identification of the contour separating the reentry and escape trajectories (among the escape energy cases) and the integration of the area bounded by the upper half escape cone and the contour in question.

For simplicity it is assumed that any trajectory with a periapsis equal to or below the atmosphere boundary (assumed here to be at 400,000 feet) will result in reentry. Thus, we are interested in the families of trajectories having constant periapses, which will be referred to as <u>isoperiapsis</u> contours.

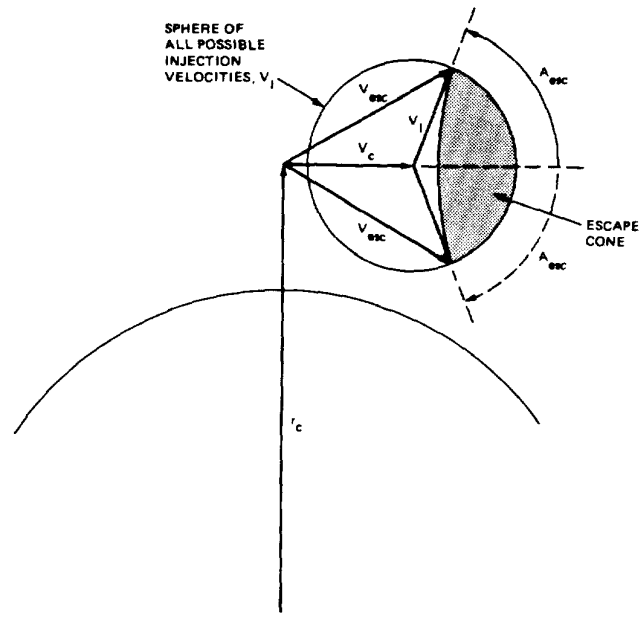

Fig. 2. The escape cone

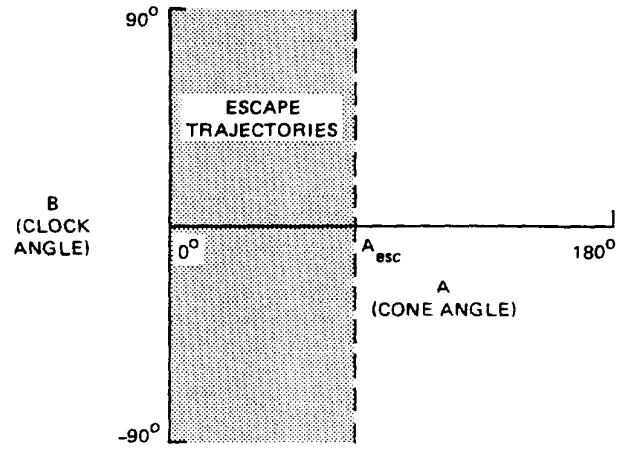

Fig. 3. Escape trajectories in the AB plane

In the next two sections, the equation of the isoperiapsis contour will be derived and the integral of the area bounded by the escape cone and the isoperiapsis contour will be specified. This integral gives the true area on the sphere of the escape trajectories for impulsive injection.

<u>The Isoperiapsis Contour in the AB Plane</u>. As discussed above, the isoperiapsis contour will be used to divide the escape cone into two regions: trajectories which escape and trajectories which reenter due to a periapsis lower than or at the atmosphere boundary.

Consider the family of trajectories with r_p = constant. The energy and angular momentum equations are

$$H = r_c V_T \cos\gamma_T = r_p V_p \tag{5}$$

$$E = (V_T^2/2) - (\mu/r_c) = (V_p^2/2) - (\mu/r_p) \tag{6}$$

where r_p and V_p are the periapsis radius and periapsis velocity, respectively. Since we are interested in isoperiapsis contours, r_p is assumed constant in Eqs. 5 and 6, but H and E are not assumed to be constant for the various families of trajectories under consideration, since V_T is a varying function of the cone angle, A:

$$V_T = \left(V_c^2 + 2V_cV_I \cos A + V_I^2\right)^{1/2} \quad (7)$$

The flight path angle, γ_T, is a function of both cone angle, A, and clock angle, B:

$$\gamma_T = \sin^{-1}\left[(V_I/V_T) \sin A \sin B\right] \quad (8)$$

Thus for isoperiapsis contours, the only two constants in Eqs. 5 and 6 are r_p and μ as the cone and clock angles A and B are permitted to vary for different injections.

Eliminating V_p from Eqs. 5 and 6 we obtain

$$(V_T^2/2)\left[1 - (r_c/r_p)^2 \cos^2 \gamma_T\right] = (\mu/r_c) - (\mu/r_p) \quad (9)$$

We will now write $V_T = V_T(A)$ and $\gamma_T = \gamma_T(A,B)$ to obtain the equation of the isoperiapsis contour in the AB plane. The result from Eqs. 7, 8 and 9 is

$$a \cos A + b = \sin^2 A \sin^2 B \quad (10)$$

where:

$$a = 2(V_c/V_I)\left[1 - (r_p/r_c)^2\right]$$

$$b = \left[1 + (V_c/V_I)^2\right]\left[1 - (r_p/r_c)^2\right] - \left(2\mu/V_I^2\right)\left(r_p/r_c\right)^2\left(r_p^{-1} - r_c^{-1}\right)$$

Let us put Eq. 10, which is the equation of the isoperiapsis contour, in the xyz coordinates of Fig. 4. Then the transformation equations for the unit sphere become

$$x = \sin A \sin B \quad (11)$$

$$y = \cos A \quad (12)$$

$$z = \sin A \cos B \quad (13)$$

So that Eq. 10 can be put in the form

$$ay + b = x^2 \quad (14)$$

Thus the equation of the isoperiapsis contours is the equation of a parabola. Figure 5 illustrates the geometric interpretation of the isoperiapsis contours: the intersection of the sphere of injection velocities with a parabolic cylinder which extends along the plus and minus z directions.

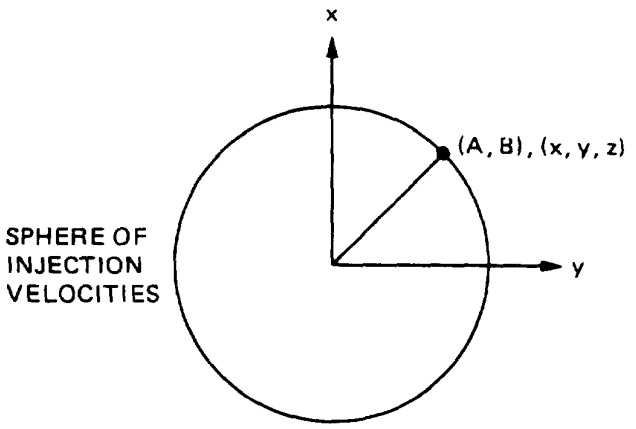

Fig. 4. Sphere of injection velocities

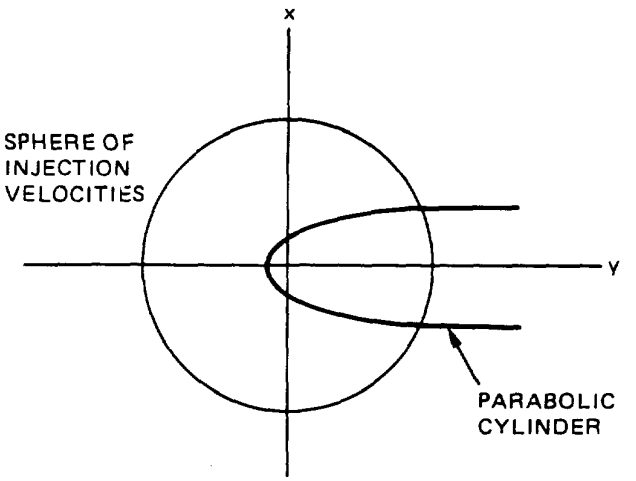

Fig. 5. Parabolic cylinder for isoperiapsis contours

Area Under the Isoperiapsis Contour. The area under the isoperiapsis contour and above the escape contour is illustrated in Figs. 6 and 7. This area corresponds to hyperbolic entries, which are trajectories with escape velocity or greater but with periapses lower than or equal to the atmosphere and with initial flight path angles that are negative.

Besides quantifying the area of hyperbolic entries, integration under the isoperiapsis contour also can be used to quantify two other areas: actual escape trajectories and orbit decay trajectories. The calculation of the area of actual escape trajectories is trivial: subtract the area of the hyperbolic entries from the area of the escape cone. The area of the orbit decay cases, illustrated in Figs. 6 and 7, involves another integration under the isoperiapsis contour and bounded by the escape cone. These are the cases in which the orbit is elliptic and the periapsis is above or at the atmosphere. All remaining cases are elliptic with periapses lower than the atmosphere and so involve prompt or delayed entries corresponding to negative and positive initial flight path angles, respectively. Some of the prompt cases are powered entries, which will be discussed in the next section.

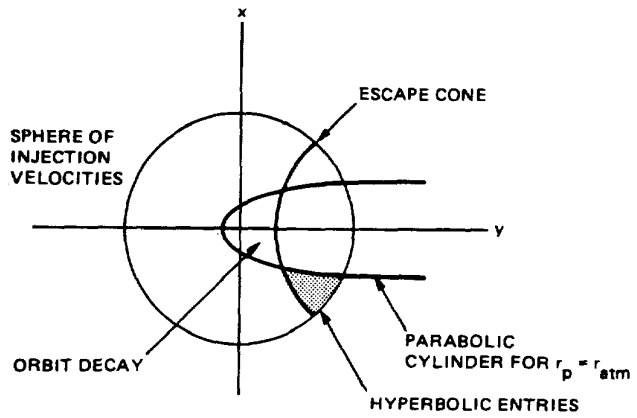

Fig. 6. Hyperbolic entries

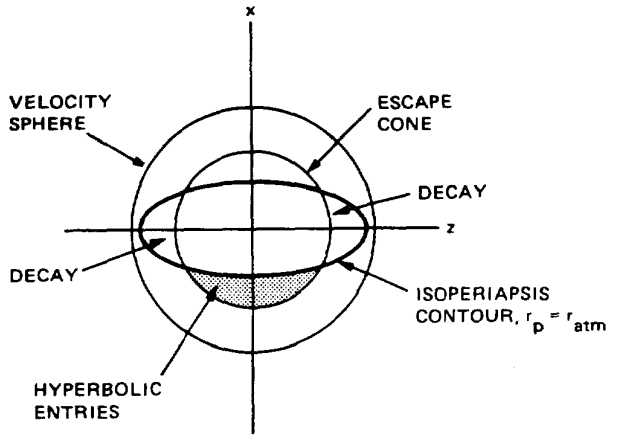

Fig. 7. Hyperbolic entries

In Fig. 8, the integration of the area between the isoperiapsis contour and the escape cone is illustrated. The shaded area corresponds to half of the hyperbolic entries. The surface integral of Fig. 8, normalized (by dividing by 4π) so that the sphere has unit area, is[1]

$$S_{hyp}/2 = (1/4\pi)\int_{A(-90°)}^{A_{esc}} \int_{B(A_{esc})}^{B(A)} \sin A \, dB \, dA \qquad (15)$$

where B(A) is found from Eq. 10:

$$B(A) = \sin^{-1}\left[(a \cos A + b)^{1/2}/\sin A\right] \qquad (16)$$

and A(-90°) is the value of A for B = -90° on the isoperiapsis contour (the inverse function of B(A)):

$$A(-90°) = \sin^{-1}\left[(a + b)^{1/2}\,(a + 1)^{-1/2}\right] \qquad (17)$$

Methods to approximate the integrals for the area of hyperbolic entries (Fig. 8) and the area of orbit decay (Fig. 9) will be discussed in the section on numerical applications (below).

The Finite-Burn, Single-Stage Problem

In the previous paper[1], Hill's Equations of Relative Motion (also referred to as the Clohessy-Wiltshire Equations), were used to analyze the single stage, finite burn problem.

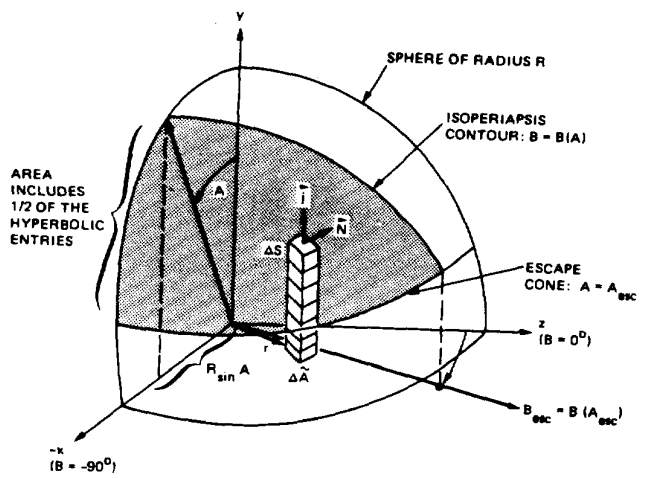

Fig. 8. Integration of hyperbolic entry area

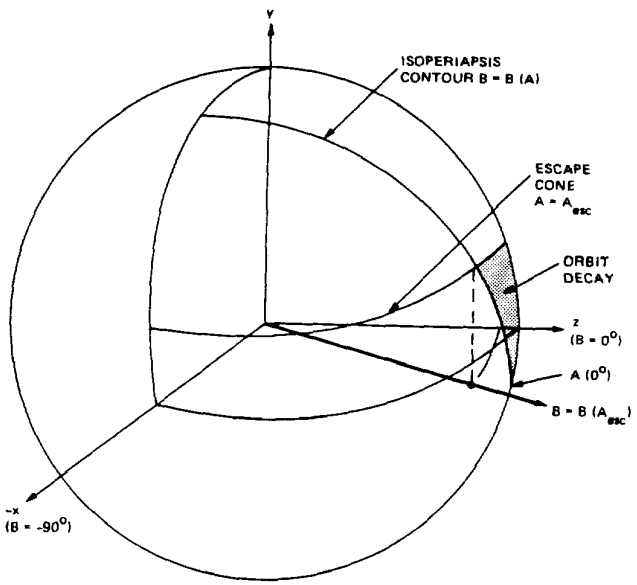

Fig. 9. Integration of orbit decay area

A modern application of Hill's Equations is to analyze the rendezvous problem. If a target vehicle in circular orbit is assumed to be at the origin of a rotating reference frame xyz which has the x axis pointing away from the center of the earth (see Fig. 10) and the y axis pointing along the circular velocity vector, then Hill's Equations, describing the motion of a rendezvous vehicle, relative to the target vehicle are as follows

$$\ddot{x} - 2n\dot{y} - 3n^2x = a_x \qquad (18)$$

$$\ddot{y} + 2n\dot{x} = a_y \qquad (19)$$

$$\ddot{z} + n^2z = a_z \qquad (20)$$

where $n = \dot{\theta} = V_c/r_c$ and a_x, a_y and a_z are accelerations from external forces (such as thrusters). An excellent discussion of these equations is presented in Kaplan[4]. Notice that even if there are no external forces, there would still be a relative acceleration between the rendezvous

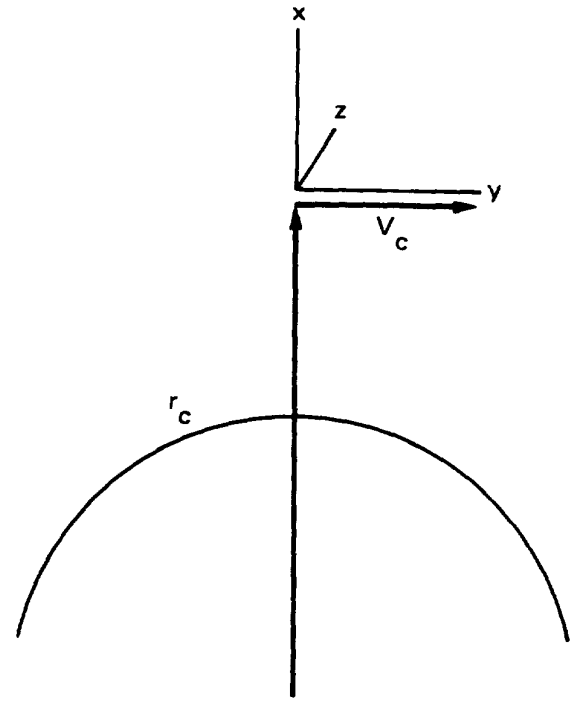

GEOMETRY

TYPICAL BEHAVIOR

Fig. 10. Relative motion

vehicle and the target (origin). This is because, in general, the vehicles are not in the same orbit. Notice also that Eq. 20 represents out-of-plane motion which is decoupled from the in-plane motion.

We will assume that the acceleration from the injection rocket will have a fixed direction in inertial space (but that the direction will be in error). Let a_X, a_Y and a_Z be the inertial accelerations. Since the xyz coordinates rotate at a rate of n, Eqs. 18-20 become

$$\ddot{x} - 2n\dot{y} - 3n^2 x = a_X \cos nt + a_Y \sin nt \tag{21}$$

$$\ddot{y} + 2n\dot{x} = a_Y \cos nt - a_X \sin nt \tag{22}$$

$$\ddot{z} + n^2 z = a_Z \tag{23}$$

In the previous paper[1] the rotational effect on the acceleration was ignored, resulting in a small error for long burns.

Note that Eq. 22 can be integrated once to obtain

$$\dot{y}(t) = \dot{y}_0 - 2n(x(t) - x_0) + \frac{a_Y}{n} \sin nt + \frac{a_X}{n} (\cos nt - 1) \tag{24}$$

Substituting Eq. 24 into Eq. 21 we obtain

$$\ddot{x} + n^2 x = 2n (\dot{y}_0 + 2nx_0) - 2a_X + 3a_Y \sin nt + 3a_X \cos nt \tag{25}$$

We can now easily integrate Eq. 25 by the usual methods to obtain

$$x(t) = \left(-3x_0 - \frac{2}{n} \dot{y}_0 + \frac{2}{n^2} a_X\right) \cos nt + \left(\frac{1}{n} \dot{x}_0 + \frac{3}{2} \frac{a_Y}{n^2}\right) \sin nt - \frac{3}{2} \frac{a_Y}{n} t \cos nt + \frac{3}{2} \frac{a_X}{n} t \sin nt + \frac{2}{n} \left(\dot{y}_0 + 2nx_0\right) - 2 \frac{a_X}{n^2} \tag{26}$$

Substituting the solution for x (Eq. 26) into Eq. 24 and integrating term by term gives the solution for y:

$$y(t) = 2 \left(3x_0 + \frac{2}{n} \dot{y}_0 - \frac{3}{n^2} a_X\right) \sin nt - \left(\frac{2}{n} \dot{x}_0 + 5 \frac{a_Y}{n^2}\right) (1 - \cos nt) + 3 \frac{a_Y}{n} t \sin nt + 3 \frac{a_X}{n} t \cos nt - 3 \left(2nx_0 + \dot{y}_0 - \frac{a_X}{n}\right) t + y_0 \tag{27}$$

The solution for z is trivial, since it is decoupled. Integrating Eq. 23, we obtain:

$$z = (z_0 - a_Z/n^2) \cos nt + (\dot{z}_0/n) \sin nt + a_Z/n^2 \quad (28)$$

With the complete solution of Hill's Equations, it is now possible to address the powered entry problem. The idea is to rendevous with the atmosphere. This means setting Eq. 26 to

$$x(t_{atm}) = x_{atm} \quad (29)$$

where

$$x_{atm} = r_{atm} - r_c \quad (30)$$

which is a negative number (approximately equal to -100 km). The time, t_{atm} is an arbitrary constant between 0 and t_b, where t_b is the total burn time. By picking $t_{atm} = t_b$, the solution of Hill's Equations gives the conditions during entry at the moment of burnout. Similarly by setting $t_{atm} = t_b/2$, the conditions at entry, when half the fuel is burned, can be examined.

It will be assumed that the initial relative positions and velocities are zero

$$x_0 = y_0 = z_0 = \dot{x}_0 = \dot{y}_0 = \dot{z}_0 = 0 \quad (31)$$

Writing out Eq. 26 gives

$$x_{atm} = \frac{a_X}{n^2}\left[2(\cos nt_{atm} - 1) + \frac{3}{2} nt_{atm} \sin nt_{atm}\right] + \frac{3}{2}\frac{a_Y}{n^2}(\sin nt_{atm} - nt_{atm} \cos nt_{atm}) \quad (32)$$

All the terms in Eq. 32 are known except the accelerations a_X and a_Y. The equation specifies the relationship between a_X and a_Y so that the vehicle will enter the atmosphere at the time t_{atm}.

Eq. 32 can be written most simply as

$$C_3 = c_1 a_X + c_2 a_Y \quad (33)$$

which is just the equation of a line, since the c's are all constants.

The value of the constant acceleration will be found through the rocket equation (see Greenwood[5]):

$$\Delta V = I_{sp} g \ln(m_o/m_f) \quad (34)$$

If incomplete burns are going to be considered ($t_{atm} < t_b$) then Eq. 34 can be written as

$$\Delta V = I_{sp} g \ln[m_o/(m_o - (m_o - m_f)(t/t_b))] \quad (35)$$

Thus, the average acceleration is

$$a = \Delta V/t = (I_{sp} g/t)\ln[m_o/(m_o - (m_o - m_f)(t/t_b))] \quad (36)$$

Now, consider a sphere of radius, a, in the xyz coordinate system (Fig. 11).

Then a plane representing Eq. 33 can be drawn through the sphere. The sphere represents all the possible accelerations that can be applied to the vehicle and the direction of the application of thrust can be specified by the cone angle, A, and clock angle, B, as in the velocity sphere (Fig. 1). Then the components of acceleration are given by

$$a_X = a \sin A \sin B \quad (37)$$

$$a_Y = a \cos A \quad (38)$$

$$a_Z = a \sin A \cos B \quad (39)$$

The points on the sphere that also satisfy Eq. 33 (the plane equation) describe a circle, which is the locus of points that result in reentry at a specified time, t_{atm}. The various loci representing various reentry times (ranging from 0 to t_b seconds) will be referred to as isochrones (for constant time contours).

Combining Eqs. 33, 37 and 38 allows the solution of the clock angle, B, as a function of the cone angle, A:

$$\sin B = (C_3 - c_2 a \cos A)/c_1 a \sin A \quad (40)$$

Thus, given a cone angle, A, a clock angle B is computed from Eq. 40 which corresponds to an isochrone circle.

This model for the isochrones has been very successful in explaining the numerically generated burn plane diagram for the single stage Galileo/Centaur problem shown in Fig. 12, as can be seen by the analytically derived Fig. 13. There is comparable agreement for the Ulysses/Centaur case.[1]

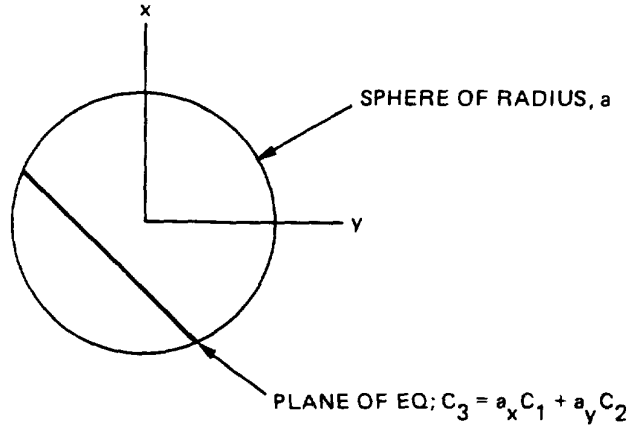

Fig. 11. Acceleration sphere

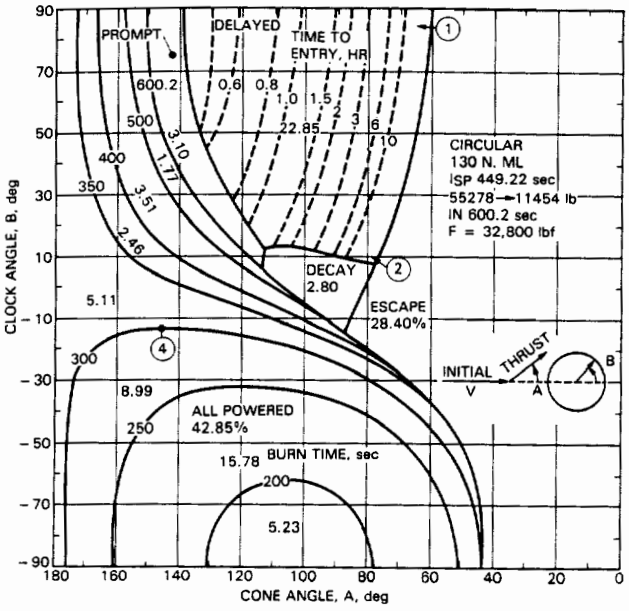

Fig. 12. Galileo/Centaur misaligned burn diagram: burn plane

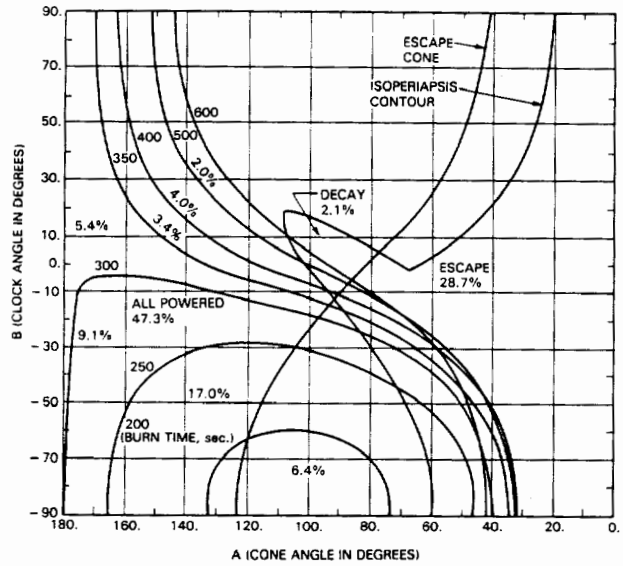

Fig. 13. Analytic solution for Galileo/Centaur burn plane

The Finite-Burn, Multi-Stage Problem

For convenience, we repeat Hill's Equations with inertially fixed accelerations (Eqs. 21 - 23):

$$\ddot{x} - 2n\dot{y} - 3n^2x = a_X \cos nt + a_Y \sin nt \qquad (41)$$

$$\ddot{y} + 2n\dot{x} = a_Y \cos nt - a_X \sin nt \qquad (42)$$

$$\ddot{z} + n^2z = a_Z \qquad (43)$$

In order to model the multi-staging we assume that the accelerations come in step functions as follows:

$$a_X = \sum_{k=1}^{m} a_{X_k} [h(t - T_{ki}) - h(t - T_{kf})] \qquad (44)$$

$$a_Y = \sum_{k=1}^{m} a_{Y_k} [h(t - T_{ki}) - h(t - T_{kf})] \qquad (45)$$

$$a_Z = \sum_{k=1}^{m} a_{Z_k} [h(t - T_{ki}) - h(t - T_{kf})] \qquad (46)$$

where

m = total number of stages

a_{X_k} = acceleration of the kth stage along the X inertial coordinate

T_{ki} = time of ignition of the kth stage

T_{kf} = burnout (or final) time of the kth stage

For the first stage, we will use Eq. 36 to model the average acceleration. For the other stages, we will assume that the average acceleration is found by

$$a_k = \Delta V_k/(T_{kf} - T_{ki}) = I_{sp_k} g \ln(m_{ki}/m_{kf})/(T_{kf} - T_{ki}) \qquad (47)$$

Integration of the z Equation

We will demonstrate our approach on the simplest equation, Eq. 43. Combining Eqs. 43 and 46, the differential equation for z is:

$$\ddot{z} + n^2z = a_{Z_k} [h(t - T_{ki}) - h(t - T_{kf})] \qquad (48)$$

We will assume zero initial conditions:

$$z(0) = \dot{z}(0) = 0 \qquad (49)$$

Care must be exercised when integrating differential equations with step functions, which are in the class of generalized function. W. Kaplan[6] discusses the theory of generalized functions in his book on operational methods.

For Eq. 48, Kaplan defines the operator $T_o[f]$ for initial values zero:

$$T_o[f] = \frac{1}{n} \int_o^t \sin n(t - u) f(u)\, du \qquad (50)$$

Putting

$$f(u) = h(u - a) \qquad (51)$$

into Eq. 50, we obtain:

$$T_o[h(t-a)] = \frac{1}{n^2}\,[1 - \cos(n\,[t-a])]\,h(t-a) \tag{52}$$

Since Eq. 48 is linear, the solution from Eq. 52 is

$$z = \sum_{k=1}^{m} a_{Z_k} \frac{1}{n^2}\left[\left\{1 - \cos(n[t - T_{ki}])\right\}h(t - T_{ki}) - \left\{1 - \cos(n[t - T_{kf}])\right\} h(t - T_{kf})\right] \tag{53}$$

Integration of the x Equation

In order to integrate Eq. 41, we must first perform a single integration of Eq. 42 to obtain y (as in the single stage problem) and then substitute the expression for y into Eq. 41 to decoupled Eqs. 41 and 42. We obtain for y:

$$\begin{aligned}\dot{y} = &- 2nx \\ &+ \frac{1}{n}\sum_{k=1}^{m} a_{Y_k}\,[(\sin nt - \sin nT_{ki})h(t - T_{ki}) \\ &- (\sin nt - \sin n\,T_{kf})h(t - T_{kf})] \\ &+ \frac{1}{n}\sum_{k=1}^{m} a_{X_k}\,[(\cos nt - \cos nT_{ki})h(t - T_{kf}) \\ &- (\cos nt - \cos nT_{kf})h(t - T_{kf})]\end{aligned} \tag{54}$$

Substituting Eq. 54 into Eq. 41 gives

$$\ddot{x} + n^2x = \sum_{k=1}^{m}\left\{a_{X_k}\,[3c(h_i - h_f) - 2(c_ih_i - c_fh_f)] + a_{Y_k}\,[3s(h_i - h_f) - 2(s_ih_i - s_fh_f)]\right\} \tag{55}$$

where we have introduced the notation

$$h_i = h(t - T_{ki}),\ h_f = h(t - T_{kf})$$

$$c = \cos nt,\ s = \sin nt$$

$$c_i = \cos nT_{ki},\ c_f = \cos nT_{kf}$$

$$s_i = \sin nT_{ki},\ s_f = \sin nT_{kf}$$

Consider the solution of

$$\ddot{x} + n^2x = f(t) \tag{56}$$

with

$$x(0) = \dot{x}(0) = 0$$

and

$$f(t) = h(t - a),$$

$$\cos nt\ h(t - a), \text{ or}$$

$$\sin nt\ h(t - a)$$

Then the operator, T_o, given by Eq. 50 gives

$$T_o\,[h(t-a)] = \frac{1}{n^2}\,\{1 - \cos n(t-a)\}\,h\,(t-a) \tag{57}$$

$$T_o\,[\cos nt\ h(t-a)] = \frac{1}{2n^2}\,\{n(t-a)\sin nt - \sin na \sin n\,(t-a)\} \cdot h(t-a) \tag{58}$$

$$T_o[\sin nt\ h(t-a)] = \frac{1}{2n^2}\,\{\sin nt - n(t-a)\cos nt - \sin na \cos n(t-a)\}\,h(t-a) \tag{59}$$

Thus, the multi-stage solution for x(t) is

$$\begin{aligned}x(t) = \frac{1}{n^2}\sum_{k=1}^{m}\Bigg\{&a_{X_k}\left[\frac{3}{2}\,(N_is - s_iS_i)h_i\right. \\ &- \frac{3}{2}\,(N_fs - s_fS_f)h_f \\ &\left.- 2\,c_i\,(1 - C_i)\,h_i + 2c_f\,(1 - C_f)\,h_f\right] \\ &+ a_{Y_k}\left[\frac{3}{2}\,(s - N_ic - s_iC_i)\,h_i\right. \\ &- \frac{3}{2}\,(s - N_fc - s_fC_f)\,h_f \\ &\left.- 2\,s_i\,(1 - C_i)\,h_i + 2s_f\,(1 - C_f)\,h_f\right]\Bigg\}\end{aligned} \tag{60}$$

where we have introduced additional notation

$$C_i = \cos n(t - T_{ki}),\ C_f = \cos n(t - T_{kf})$$

$$S_i = \sin n(t - T_{ki}),\ S_f = \sin n(t - T_{kf})$$

$$N_i = n(t - T_{ki}),\ N_f = n(t - T_{kf})$$

Integration of the y Equation

By substituting Eq. 60 into Eq. 54 and integrating, we obtain y(t):

$$y(t) = \frac{1}{n^2} \sum_{k=1}^{m} \Big\{ a_{X_k} [3(N_i c - s + s_i)h_i - 3(N_f c - s + s_f)h_f + 3s_i(1 - C_i)h_i - 3s_f(1 - C_f)h_f + 3(c_i N_i h_i - c_f N_f h_f) - 4(c_i S_i h_i - c_f S_f h_f) + (s - s_i)h_i - (s - s_f)h_f] + a_{Y_k} [2(c - c_i)h_i - 2(c - c_f)h_f + 3(N_i s + c - c_i)h_i - 3(N_f s + c - c_f)h_f - s_i S_i h_i + s_f S_f h_f + 3(s_i N_i h_i - s_f N_f h_f)] \Big\} \quad (61)$$

The Isochrone Contour. By setting the altitude equation, Eq. 60, equal to the altitude of the atmosphere at a given time, we obtain the equation of isochrone (fixed time) contours:

$$x(t_{atm}) = x_{atm} \quad (62)$$

Eq. 60 can be put in the form:

$$x(t_{atm}) = \sum_{k=1}^{m} a_{X_k} f_{X_k}(t_{atm}) + a_{Y_k} f_{Y_k}(t_{atm}) \quad (63)$$

Suppose that the initial stage direction is given (a_{X_1}, a_{Y_1}, a_{Z_1}) and that the directions of the succeeding stages are determined by the first stage direction. Then Eq. 63 can be rewritten as

$$x(t_{atm}) = a_{X_1} \sum_{k=1}^{m} \bar{a}_{X_k} f_{X_k}(t_{atm}) + a_{Y_1} \sum_{k=1}^{m} \bar{a}_{Y_k} f_{Y_k}(t_{atm}) \quad (64)$$

where we have introduced the scaled accelerations

$$\bar{a}_{X_k} = a_{X_k}/a_{X_1} \quad (65)$$

$$\bar{a}_{Y_k} = a_{Y_k}/a_{Y_1} \quad (66)$$

and where $\bar{a}_{X_1} = \bar{a}_{Y_1} = 1$. We assume that the scaled variables in Eqs. 65 and 66 are known parameters.

If we define new functions

$$g_X(t_{atm}) = \sum_{k=1}^{m} \bar{a}_{X_k} f_{X_k}(t_{atm}) \quad (67)$$

$$g_Y(t_{atm}) = \sum_{k=1}^{m} \bar{a}_{Y_k} f_{Y_k}(t_{atm}) \quad (68)$$

then

$$x(t_{atm}) = a_{X_1} g_X(t_{atm}) + a_{Y_1} g_Y(t_{atm}) \quad (69)$$

Since g_X and g_Y are known functions of t_{atm}, Eq. 69 is the equation of a line as before in the single stage case. In our application to the Galileo and Ulysses problems we assume the directions of all the stages will be the same.

Eq. 69 not only applies to these problems, but also cases in which the succeeding stages are misaligned in a different fixed directions. Thus the linear equation of Eq. 69 is an important general result.

The Velocity Components

The velocity component in xyz coordinates are given by

$$V_x = \dot{x} \quad (70)$$

$$V_y = \dot{y} + V_c + nx \quad (71)$$

$$V_z = \dot{z} \quad (72)$$

A convenient expression for y is found in Eq. 54. The expressions for x and z are found by differentiating Eqs. 60 and 53. (Note: the delta functions which arise from differentiation are of no consequence to physical systems[6] and so will be ignored.)

$$\dot{x}(t) = \frac{1}{n} \sum_{k=1}^{m} \Big\{ a_{X_k} \Big[\frac{3}{2}(s + N_i c - s_i C_i) h_i - \frac{3}{2}(s + N_f c - s_f C_f) h_f - 2(c_i S_i h_i - c_f S_f h_f) \Big] + a_{Y_k} \Big[\frac{3}{2}(N_i s + s_i S_i) h_i - \frac{3}{2}(N_f s + s_f S_f) h_f - 2(s_i S_i h_i - s_f S_f h_f) \Big] \Big\} \quad (73)$$

$$\dot{z}(t) = \frac{1}{n}\sum_{k=1}^{m} a_{Z_k}[S_i h_i - S_f h_f] \qquad (74)$$

Simplified Velocity Equations. Eqs. 70-74 and 54 specify the velocity for the multi-stage problem, but they are very difficult to work with. In order to guide future work, a simplified approach is provided now.

Let us assume that the altitude remains constant during the burn and that the acceleration maintains a constant direction in inertial space. We will also assume that the circular velocity of the initial orbit rotates at a constant angular rate (n) and can be added to the accrued velocity of the vehicle. Then for this highly simplified model, the inertial components are

$$V_X = a_X t - V_c \sin nt \qquad (75)$$

$$V_Y = a_Y t + V_c \cos nt \qquad (76)$$

$$V_Z = a_Z t \qquad (77)$$

Let $\Delta V_X = a_X t$, $\Delta V_Y = a_Y t$ and $\Delta V_Z = a_Z t$ so that Eqs. 75-77 become

$$V_X = \Delta V_X - V_c \sin nt \qquad (78)$$

$$V_Y = \Delta V_Y + V_c \cos nt \qquad (79)$$

$$V_Z = \Delta V_Z \qquad (80)$$

Notice that when t = 0 in Eqs. 78-80 we have the impulsive injection case. Thus, the effect of Eqs. 78-80 is to include the rotation of the circular velocity vector. The effect on the escape cone and the isoperiapsis contour is simply to rotate the coordinate system by an angle of nt, where the time, t, is now interpreted to be the total time from first ignition to final burnout, including coast times in between.

With these simplified expressions for velocity (Eqs. 78-80) the areas for escape, hyperbolic entry and orbit decay reduce to that of the impulsive injection case. In the numerical applications (below) it will be demonstrated that these approximations are reasonably good. It can also be demonstrated analytically that for nt small, Eqs. 75-77 are obtained from the multi-stage equations.

Numerical Applications

We will now apply the multi-stage models developed above to the Galileo-IUS and the Ulysses-IUS problems. For the escape trajectories we will approximate the area by

$$S_{esc} \approx f(1 - \cos A_{esc})/2 \qquad (81)$$

where

$$f = 1/2 + 1/\pi\,(\alpha + \sin\alpha \cos\alpha)$$

$$\alpha = \sin^{-1}(A(-90°)/A_{esc}) \text{ in radians}$$

and where A (-90°) is defined by Eq. 17. (See Fig. 14)

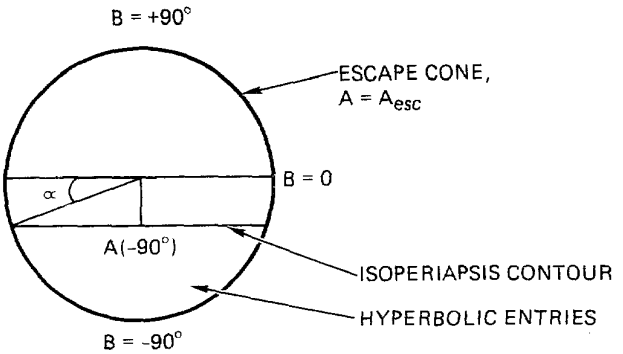

Fig. 14. Approximation for escape trajectories

As in Ref. 1, spherical triangles will be used to approximate the area of orbit decay, since for low Earth orbits, the isoperiapsis contour can be approximated by great circles.

In Fig. 15, the numerical results are shown for the Galileo burn plane for an orbital altitude of 110 NM. In Fig. 16 the analytic model is applied to the same problem.

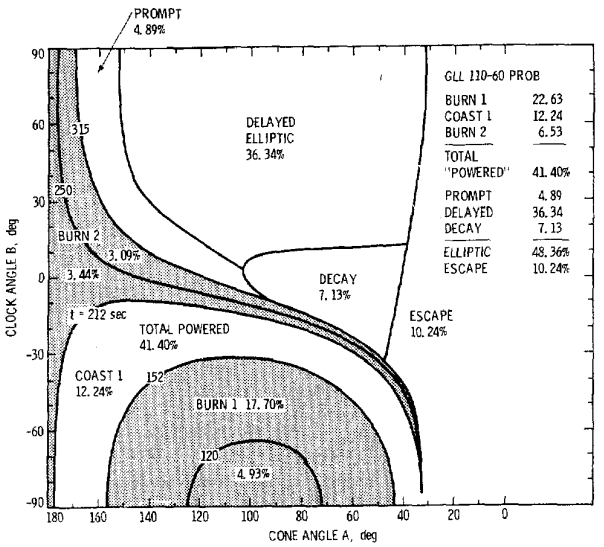

Fig. 15. Fixed misdirected burn map for Galileo (numerical solution) for 110 NM orbit

Table 1 gives the burn durations, masses and I_{sp}'s.

The area for the delayed entries is approximated by (1-H-D)/2 where H is the area of the escape cone and D is the area of the delay. No value is obtained for the prompt trajectories. Because of the slightly overestimated area for the total powered entries, the total of powered, elliptic and escape is slightly over 100% for the analytic solutions. We also note that the escape cone and isoperiapsis contours of the analytic solution are rotated by a greater angle than their counterparts in the numerical solution. In spite of this, there is very good agreement for the percentage of escapes and good agreement for the percentage of decays.

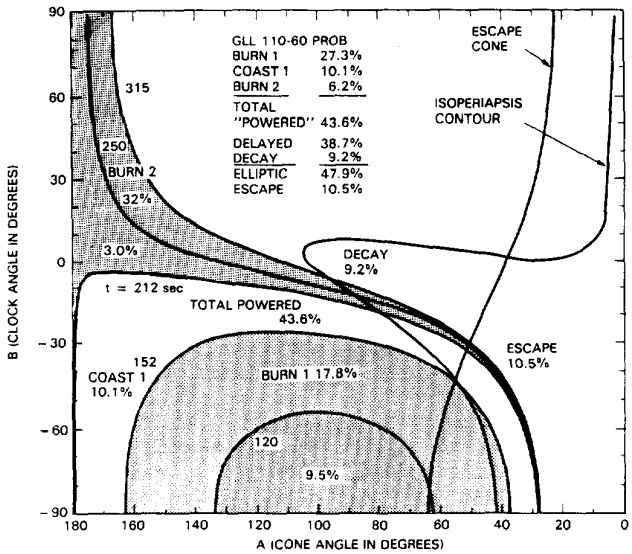

Fig. 16. Fixed misdirected burn map for Galileo (analytic solution) for 110 NM orbit

Table 1. Galileo Injection at 110 NM

Event	Time, sec	Mass, lb	I_{sp}, sec
BURN 1	0-152	38676-17033	293.3
COAST 1	152-212		
BURN 2	212-315.4	14593-8519	301.2

Table 2 presents the data used for Galileo injection at 160 NM with a burn delay between the first and second stages of 200 seconds.

Table 2. Galileo Injection at 160 NM

Event	Time, sec	Mass, lb	I_{sp}, sec
BURN 1	0-152	38676-17033	293.3
COAST 1	152-352		
BURN 2	352-455.4	14693-8519	301.2

The numerical and analytic solutions are shown in Figs. 17 and 18, respectively.

For Ulysses, which involves three stages, Tables 3 and 4 give the burn parameters for initial orbits of 110 NM and 160 NM. The numerical and analytic results are displayed in Figs. 19-22.

In each figure we see that the analytic models capture the essential behavior of the burn plane. The average discrepancy between the numerical and analytic approaches is a few percent, with the greatest differences occurring for the minimum time for powered entries. (Of course this is where we expect the greatest differences to show, because there must be some cases where the analytic solution would just barely predict reentry, while the numerical case would not.) In general the analytic solution tends to overestimate the powered entries.

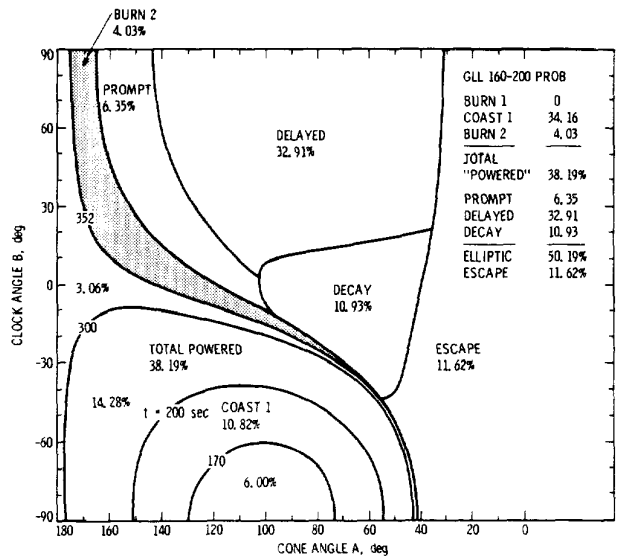

Fig. 17. Fixed misdirected burn map for Galileo (numerical solution) for 160 NM orbit

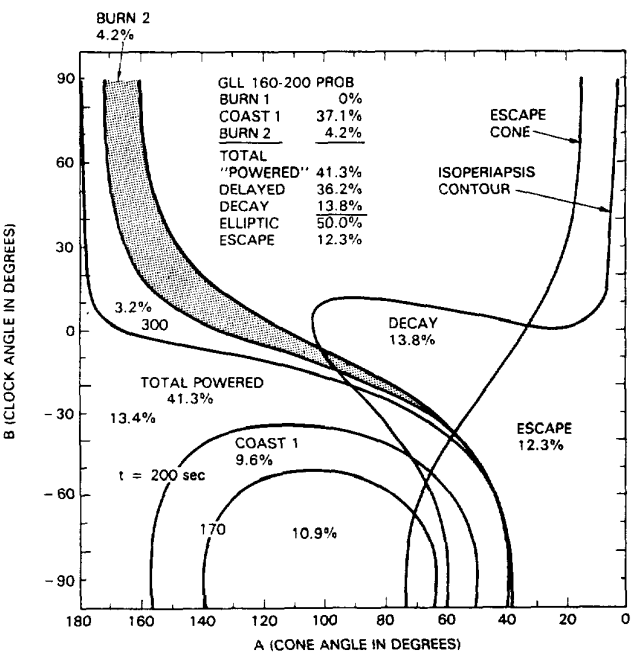

Fig. 18. Fixed misdirected burn map for Galileo (analytic solution) for 160 NM orbit

Table 3. Ulysses Injection at 110 NM

Event	Time, sec	Mass, lb	I_{sp}, sec
BURN 1	0-152	38676-17033	293.3
COAST 1	152-212		
BURN 2	212-315.4	14593-8519	301.2
COAST 2	315.4-375.4		
BURN 3	375.4-460.4	5914-1415	292.1

Table 4. Ulysses Injection at 160 NM

Event	Time, sec	Mass, lb	I_{sp}, sec
BURN 1	0-152	38676-17033	293.3
COAST 1	152-352		
BURN 2	352-455.4	14593-8519	301.2
COAST 2	455.4-656.4		
BURN 3	655.4-740.4	5914-1415	292.1

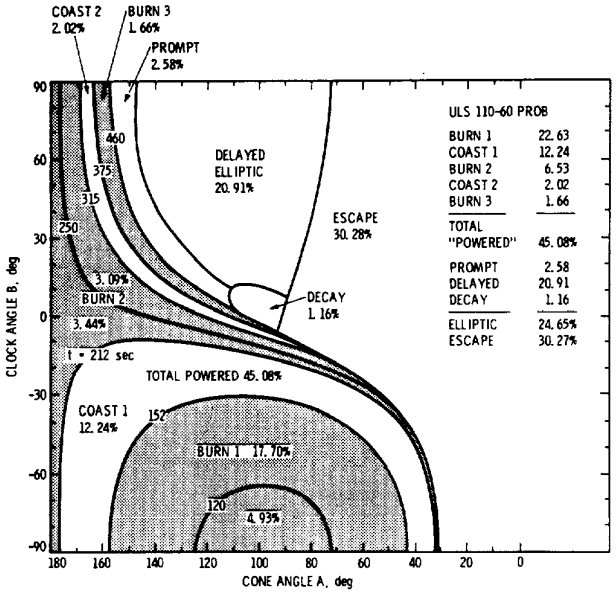

Fig. 19. Fixed misdirected burn map for Ulysses (numerical solution) for 110 NM orbit

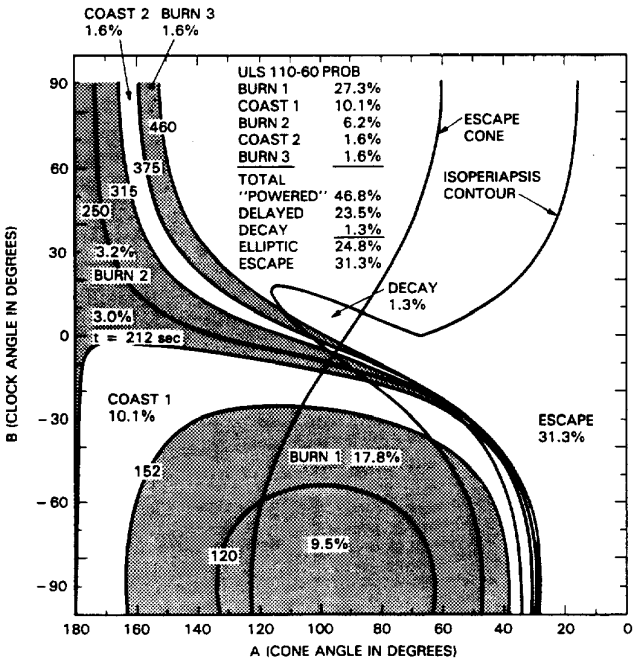

Fig. 20. Fixed misdirected burn map for Ulysses (analytic solution) for 110 NM orbit

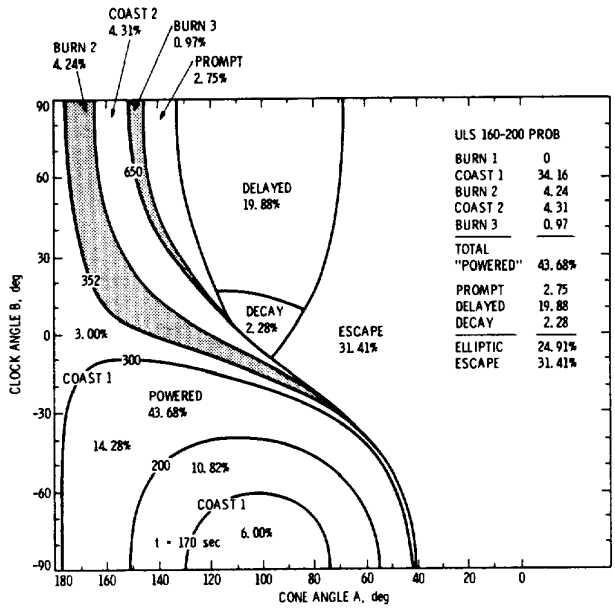

Fig. 21. Fixed misdirected burn map for Ulysses (numerical solution) for 160 NM orbit

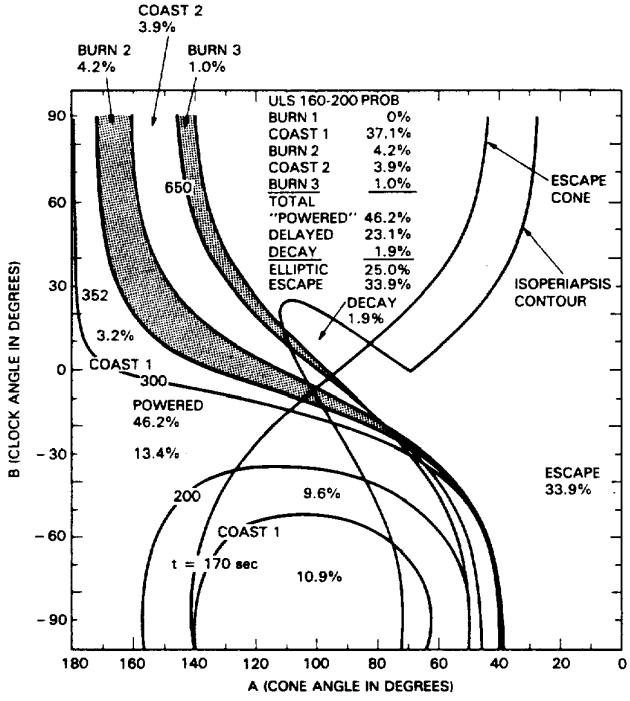

Fig. 22. Fixed misdirected burn map for Ulysses (analytical solution) for 160 NM orbit

Conclusions

An analytic model has been developed for the multi-stage injection problem. It shows good agreement with numerically generated plots and simplifies the analysis considerably. Both methods have their disadvantages and sources of

error. The analytic method is limited by the linearized equations and other simplifying assumptions necessary to make the problem tractable. In the numerical approach the accuracy is limited by the number of points selected on the burn plane for simulation, which is limited by the time (and patience) of the analyst. Because of these considerations, it is highly likely that both techniques have errors of the order of a few percent.

Perhaps the most profitable use of time is to use both methods in conjunction. The analytic burn plane can be produced first and requires only a few minutes to compute and plot. The results can be used to guide the selection of burn plane points in the numerical solution. Since the isochrones and the escape cone are approximated by small circles, a few one-dimensional searches in the burn plane may suffice to identify their locations and size. A similar approach may be used for the isoperiapsis contour. For small circles, numerical integration of the area is unnecessary. The area is found by measuring the radius of the circle and applying a simple formula.

In conclusion, the labor involved in the two-dimensional search on the burn plane can be reduced considerably in the numerical approach by utilizing the analytic and geometric models developed here.

Acknowledgements

The authors thank Jean-Paul Berthias, Roger Diehl, Peter Jaffe, and Robert Mitchell for their valuable support.

References

1. Longuski, J. M., "An Analytic-Geometric Model of the Effect of Spherically Distributed Injection Errors for the Galileo and Ulysses Spacecraft," AAS Paper 87-487, AAS/AIAA Astrodynamics Specialist Conference, Kalispell, Montana, August 10-13, 1987.
2. McRonald, A. D., "Galileo RTG Reentry Breakup Analysis," JPL Document 1625-228, September 1984.
3. Jaffe, P., Diner, A., McRonald, A., and Tenn, L., "Ulysses Breakup Analysis Final Report," JPL Document 1628-54, November 1984.
4. Kaplan, M. H., Modern Spacecraft Dynamics & Control, John Wiley & Sons, New York 1976.
5. Greenwood, D. T., Principles of Dynamics, Prentice-Hall, Inc., Englewood Cliffs, New Jersey, 1965.
6. Kaplan, W., Operational Methods for Linear Systems, Addison-Wesley Publishing Co., Inc., Reading, Mass., 1962.